2018 EAGE ANNUAL
80TH CONFERENCE + EXHIBITION
COPENHAGEN | DENMARK

We P8 09

Seismic Noise Characterization at a Potential Site for the Einstein Telescope Underground Gravitational Wave Detector

S. Koley (National Institute for Subatomic Physics), X. Campman (Shell Global Solutions International BV), M. Bader (National Institute for Subatomic Physics), H.J. Bulten (National Institute for Subatomic Physics), J.V.D. Brand (National Institute for Su

Summary

With the first detection of gravitational waves on September 14, 2015 and subsequent detection of four other binary black hole mergers, significant efforts have been made to improve the detector sensitivity especially at low frequencies. Seismic noise and its gravitational counterpart Newtonian noise are the two main factors limiting the sensitivity at frequencies below 20 Hz. Einstein Telescope is a European project for constructing a third generation gravitational wave detector with an effort to increasing its sensitivity at low frequencies. The detector is to be built 300 m underground to reduce the impact of seismic and Newtonian noise. Limburg, Netherlands is one of the sites for the project. Understanding the spatio-spectral properties of seismic noise at the site and the geology of the area is vital for devising schemes for simulation of seismic and Newtonian noise at desired depths. In this paper we report the results of a reconnaissance passive seismic survey, conducted at the site. Array based methods like beamforming, and seismic interferometry is used to understand the propagation characteristics of the seismic noise in the frequency range 2.5-8.0 Hz. The estimated Rayleigh wave phase velocity is further used to invert for a 1D S-wave velocity model.

Introduction

Gravitational wave (GW) detectors work on the principle of a power recycled Michelson interferometer (Saulson, 1994). One of the several noise sources limiting the sensitivity of current ground based gravitational wave detectors is seismic in origin. Ground motion of the subsurface beneath the suspended elements (mirror and beamsplitter) of the detector couples to it through the gravitational force of attraction. This causes a change in the equilibrium position of the test masses. The error introduced in the gravitational wave signal due to this change in the position of the test masses, is termed as the gravity gradient noise or the Newtonian noise (Hughes and Thorne, 1998). Typically GW detectors are shielded mechanically from seismic noise above 10 Hz using advanced techniques in seismic isolation. However, the nature of coupling of Newtonian noise prevents it from getting shielded.
Einstein Telescope (ET) is a European project for a third generation GW detector. The sensitivity of this detector will be increased by about a factor of 10 in amplitude compared to the existing Advanced Virgo and LIGO detectors, and its detection band will be extended at low frequencies to 1 Hz as shown in Figure 1(a). In order to reduce the effect of seismic and Newtonian noise, ET will be built 200 to 300 m underground. Limburg, Netherlands is one of the sites selected for the construction of the ET. Using a 1D velocity model from borehole data in the region, magnitude of surface waves corresponding to the fundamental mode and the first overtone were computed as a function of depth and frequency. Figure 1(b) and 1(c) shows the the reduced contribution of high frequency seismic noise at depths > 100 m, which further supports the theory of benefiting from building it underground. In this paper we report the results of a passive seismic study conducted at the ET site. We make use of array based analysis techniques like beamforming and seismic interferometry for understanding the spatio-spectral characteristics of the seismic noise at the site. Subsequently the estimated Rayleigh wave phase velocity dispersion is used to compute a shallow 1D S-wave velocity model of the region.

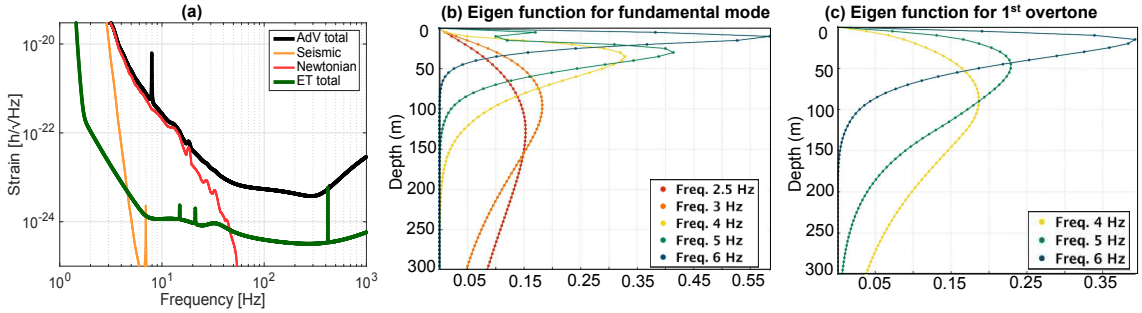

Figure 1 *(a) Advanced Virgo sensitivity curve (black) and corresponding noise contributions and Einstein Telescope sensitivity curve (green). (b) Rayleigh wave sensitivity kernel plotted as function of depth and frequency for the fundamental mode and (c) the first overtone.*

Seismic Array Design

We follow the method proposed by Woods and Lintz (1973) and use the theoretical array response as a measure for designing an array capable of resolving events in the frequency range 2.5 - 8.0 Hz. An array of 74 vertical component 4.5 Hz wireless geophones were deployed at site between November 3-16, 2017, as shown in Figure 2(a) and (b). Array A comprises 7 rings of sensors with radius increasing as $r_0 2^{n-1}$, where r_0 is selected as 3.5 m, and $n = [2,3,4,5,6,7]$. The n^{th} ring has $2n-1$ sensors equally spaced in azimuth, with 1 sensor at the center of the array. The minimum and maximum aperture of array A is 3.5 m and 456 m respectively. Array B is similar to A, but with only 5 rings and hence a maximum aperture of 112 m. Array B due to its smaller aperture has good resolving power only at frequencies > 3.4 Hz, unlike array A which has good resolution down to 2.5 Hz. Our maximum frequency of interest is 8 Hz and both arrays show no spatial aliasing. As a test of the sensor performance we compared the average power spectral density (PSD) of the data for November 11, 2017 between 4 of the sensors (marked in Figure 2(b)) to that of the nearby Heimansgroeve observatory (station HGN). Figure 2(c) shows a good coherence in the frequency band 0.2-1.5 Hz. Below 0.2 Hz, our sensors have very low sensitivity and the noise spectrum is dominated by digital noise of the recorder. At frequencies > 2 Hz, the HGN station spectrum is significantly lower than those measured by our sensors. This is because the

HGN station measures the ground motion at the bedrock level and not at the surface.

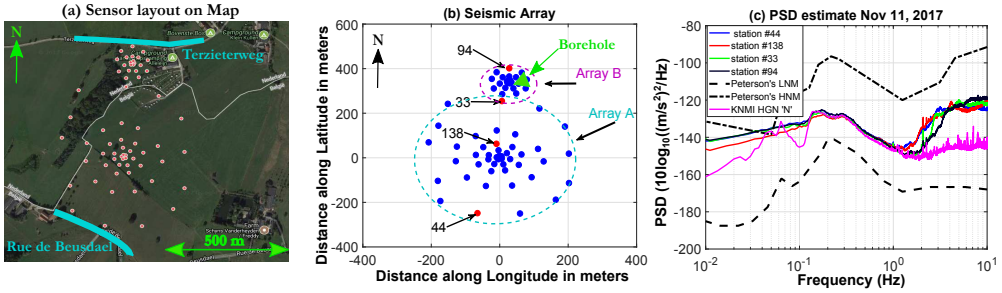

Figure 2 *(a) Array layout on a map. (b) Sensor locations in cartesian coordinates along with the location of the borehole. (c) Comparison of PSD of the 4 stations marked red in (b) and at the HGN station.*

Rayleigh wave phase velocity

In order to estimate the Rayleigh wave phase velocity and the noise propagation direction, a frequency domain beamforming method is employed. Conventional beamforming methods based on Lacoss et al. (1969) makes use of the data covariance matrix to obtain the power associated with different steering vectors. The power of the stacked signal essentially gives us information about the correctness of the delay applied and is often referred to as the beampower. The Beampower $BP(f)$ at frequency f, corresponding to a steering vector $a_k(f)$ is computed as,

$$BP(f) = a_k^*(f) R_{xx}(f) a_k(f) \tag{1}$$

where, $R_{xx}(f) = X(f)X^*(f)$ is the data covariance matrix and $a_k(f)$ is the array response vector corresponding to the k^{th} value of slowness p_k and azimuth ϕ_k. The value of (p_k, ϕ_k) corresponding to the maximum beampower gives an estimate of the slowness and the dominant noise propagation direction at that frequency.

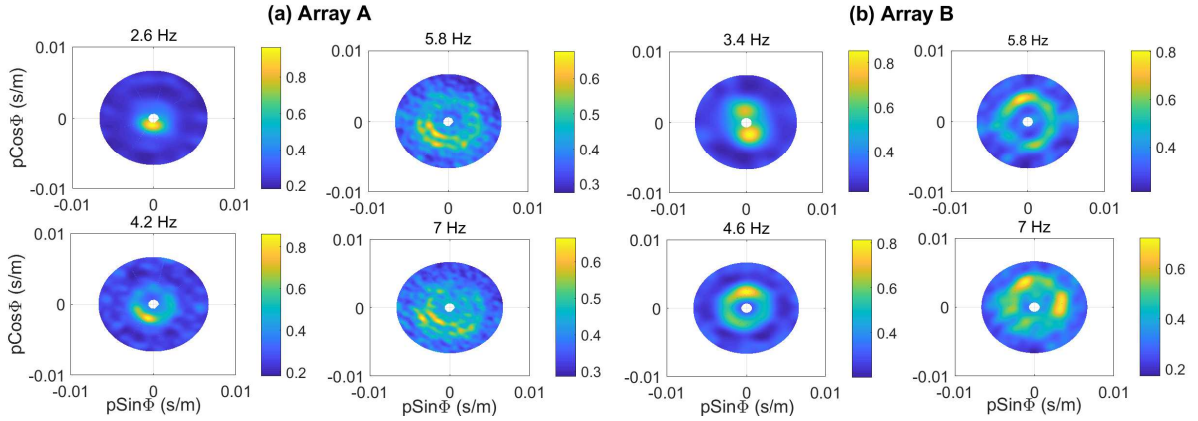

Figure 3 *Beamforming output showing normalized beampower as a function of slowness and azimuth averaged over all days of measurement between November 3-16, 2017 (a) for array A at f = 2.6, 4.2, 5.8, 7 Hz and (b) for array B at f = 3.4, 4.6, 5.8, 7 Hz.*

Beamforming was performed on two weeks of continuous noise recording at frequencies between 2.6 - 8.0 Hz. Beampower was estimated at frequency intervals of 0.1 Hz. Figure 3(a) and 3(b) shows the beampower for array A and B respectively at different frequencies. In these plots, slowness increases radially outwards and azimuth is measured anticlockwise from x-axis. Hence the x, y axis are labeled as $pCos\phi$ and $pSin\phi$ respectively. At frequencies between 2.6 - 8.0 Hz dominant noise was observed to propagate from the south-west direction originating from the road Rue de Beusdael. As we move north towards the smaller array B, noise originating from south still dominates the beampower at low frequencies, but at higher frequencies the road Terzieterweg running just north of array B becomes more

prominent (Figure 3(b)). An outcome of the beamforming method is also the phase velocity estimate, that is computed by summing up the beampower across all azimuths. Beampower is then expressed only as function of slowness. Figure 4(a) and 4(b) shows the estimated Rayleigh wave phase velocity in the frequency range of interest pertaining to array A and B respectively. In addition to the fundamental mode, the first overtone is observed for array A at frequencies > 5.6 Hz. Generally the first overtone is sensitive to deeper structures, but due to its presence at higher frequencies, its impact on the seismic noise is only limited to shallow depths (Figure 1(c)).

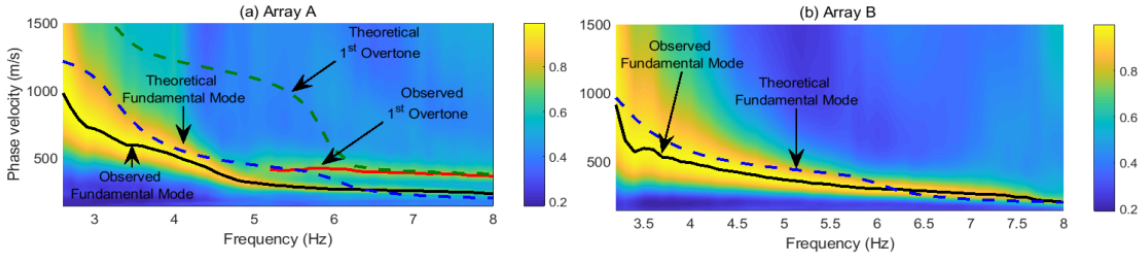

Figure 4 *Theoretical and observed dispersion curve using beamforming on (a) array A and (b) array B.*

Seismic interferometry

Following the principle of seismic interferometry (Wapenaar and Fokkema, 2006) the empirical Green's function was retrieved for all station pairs, pertaining to two weeks of continuous noise data. Data preprocessing was performed following Bensen et al. (2007). We use the interferometry results for understanding the dependence of the signal to noise ratio (SNR) of the extracted Green's function on interstation azimuth and distance in order to understand the impact of noise directionality on a future tomography study. Figure 5(a) shows a virtual noise record computed with respect to station number 33 (Figure 2(b)). Stations south of sensor 33 are assigned negative offsets and those north are assigned positive offsets. Correlation peaks are observed at causal times for stations south of the reference sensor. Sensors located north of it have correlation peaks at both causal and acausal time lags. While the correlation peaks at acausal time lags is due to the noise originating from the south, the correlation peaks at causal time lags is due to the noise originating from the road Terzieterweg running north of array B (Figure 2(a)). Figure 5(b) shows the SNR of the empirical Green's function (EGF) as a function of interstation azimuth and the distance, computed using a bin size of 10 degrees in azimuth and 40 m in interstation spacing. For each bin of station separation, maximum SNR was observed for inter-station azimuth between 60 - 100 degrees. These observations are in good agreement with the beamforming results, where a dominant noise from south-southwest was observed.

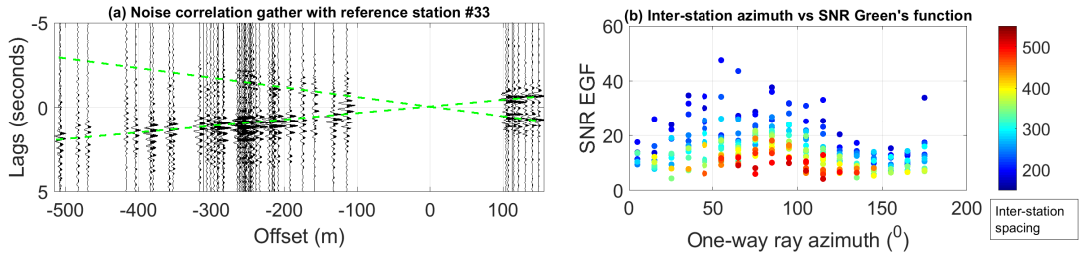

Figure 5 *(a) A noise correlation gather with station #33 as the reference sensor. (b) SNR of the empirical Green's function as a function of interstation azimuth and distance.*

Dispersion Curve Inversion

The Rayleigh wave phase velocity curve is inverted to obtain a 1D S-wave velocity model. The inversion is carried out using a stochastic direct search method as proposed in Wathelet et al. (2004). Prior to this survey, a 170 m deep borehole was dug near array B, as shown by the green triangle in Figure 2(b). It provides valuable a priori information for constraining the inverse problem. The inversion is performed for a 6 layer model (including half space) of known density and depths. The inversion perturbs only the

P and S wave-velocities of the layers, and minimizes the misfit between the theoretical and observed dispersion curves. From the inversion results, a sharp velocity contrast is observed around 40 m where the soft soil transitions into the Paleosol formation. Figure 6 shows P and S-wave velocity models visited during the inversion process.

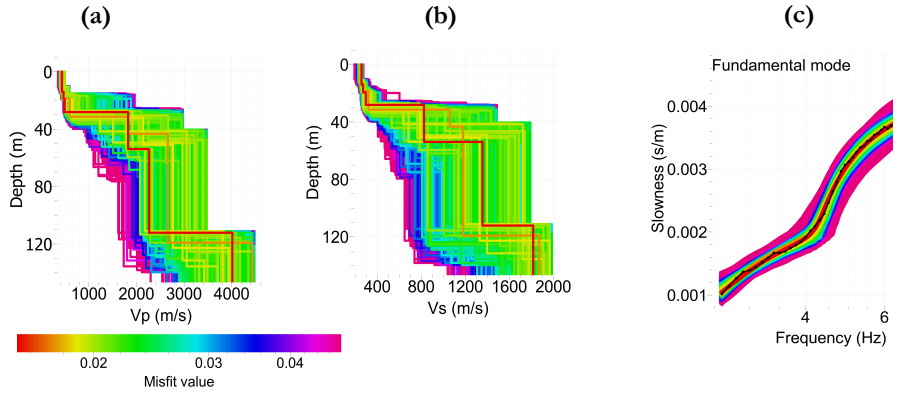

Figure 6 *(a),(b) P and S-wave velocity models explored by the algorithm during dispersion curve inversion, (c) Observed (black) and theoretical dispersion curves corresponding to all the visited models. The relative misfit values for each of these models are shown in the colorbar.*

Conclusion

In this paper, we demonstrated the use of seismic surface wave methods for understanding the propagation characteristics of seismic noise (2.5 - 8.0 Hz) at the Einstein Telescope site. The Rayleigh wave fundamental mode was observed for all frequencies of interest and the first overtone at frequencies greater than 5.6 Hz. In addition to understanding the noise illumination direction, an accurate estimation of S-wave velocity model was possible. Since this array suffers from poor ray count for longer interstation paths, a dense array of 200 geophones is currently deployed at the site with an aim of performing passive seismic tomography. A 3D velocity model would further contribute to better understanding of geology of the region and as well as more accurate simulation of the Newtonian noise.

Acknowledgements

We would like to thank NWO and Shell Global Solutions International BV[1] for funding this research and Innoseis BV for their contribution to the development of wireless geophones. We would also like to thank Mike Danilouchkine[1] for providing the sensitivity kernel plots.

References

Bensen, G., Ritzwoller, M., Barmin, M., Levshin, A., Lin, F., Moschetti, M., Shapiro, N. and Yang, Y. [2007] Processing seismic ambient noise data to obtain reliable broad-band surface wave dispersion measurements. *Geophysical Journal International*, **169**(3), 1239–1260.

Hughes, S.A. and Thorne, K.S. [1998] Seismic gravity-gradient noise in interferometric gravitational-wave detectors. *Physical Review D*, **58**(12), 122002.

Lacoss, R.T., Kelly, E.J. and Toksöz, M.N. [1969] Estimation of seismic noise structure using arrays. *Geophysics*, **34**(1), 21–38.

Saulson, P.R. [1994] *Fundamentals of interferometric gravitational wave detectors*. World Scientific.

Wapenaar, K. and Fokkema, J. [2006] Green's function representations for seismic interferometry. *Geophysics*, **71**(4), SI33–SI46.

Wathelet, M., Jongmans, D. and Ohrnberger, M. [2004] Surface-wave inversion using a direct search algorithm and its application to ambient vibration measurements. *Near surface geophysics*, **2**(4), 211–221.

Woods, J.W. and Lintz, P.R. [1973] Plane waves at small arrays. *Geophysics*, **38**(6), 1023–1041.